PAPER

Dynamic lung behavior under high G acceleration monitored with electrical impedance tomography

IOP Publishing Physiol. Meas. 42 (2021) 094001 https://doi.org/10.1088/1361-6579/ac1c63

Physiological Measurement

IPEM Institute of Physics and Engineering in Medicine

RECEIVED
13 April 2021

REVISED
4 August 2021

ACCEPTED FOR PUBLICATION
10 August 2021

PUBLISHED
27 September 2021

PAPER

Dynamic lung behavior under high G acceleration monitored with electrical impedance tomography

Tobias Menden[1], Gema B Alcaín[1], Alec T Stevenson[2], Ross D Pollock[2,3], Henry Tank[2], Peter Hodkinson[3], Caroline Jolley[3], Thomas G Smith[3], Steffen Leonhardt[1] and Marian Walter[1]

[1] Medical Information Technology (MedIT), Helmholtz-Institute for Biomedical Engineering, RWTH Aachen University, Pauwelsstr. 20, D-52074 Aachen, Germany
[2] QinetiQ, Farnborough, United Kingdom
[3] Centre for Human and Applied Physiological Sciences, King's College London, United Kingdom

E-mail: menden@hia.rwth-aachen.de

Keywords: human centrifuge, ventilation shift, tidal breathing, hypoxia, EIT, suborbital commercial spaceflight

Abstract

Objective. During launch and atmospheric re-entry in suborbital space flights, astronauts are exposed to high G-acceleration. These acceleration levels influence gas exchange inside the lung and can potentially lead to hypoxaemia. The distribution of air inside the lung can be monitored by electrical impedance tomography. This imaging technique might reveal how high gravitational forces affect the dynamic behavior of ventilation and impair gas exchange resulting in hypoxaemia. *Approach*. We performed a trial in a long-arm centrifuge with ten participants lying supine while being exposed to $+2$, $+4$ and $+6$ G_x (chest-to-back acceleration) to study the magnitude of accelerations experienced during suborbital spaceflight. *Main results*. First, the tomographic images revealed that the dorsal region of the lung emptied faster than the ventral region. Second, the ventilated area shifted from dorsal to ventral. Consequently, alveolar pressure in the dorsal area reached the pressure of the upper airways before the ventral area emptied completely. Finally, the upper airways collapsed and the end-expiratory volume increased. This resulted in ventral gas trapping with restricted gas exchange. *Significance*. At $+4$ G_x, changes in ventilation distribution varied considerably between subjects, potentially due to variation in individual physical conditions. However, at $+6$ G_x all participants were affected similarly and the influence of high gravitational conditions was pronounced.

1. Introduction

The human respiratory system is responsible for gas exchange, which takes place in the alveoli of the lung. Lung volume changes during breathing, with inflation actively driven by the diaphragm and intercostal muscles, while deflation occurs passively under the weight of the chest wall and elastic recoil. The lung and its mechanics are highly gravity-dependent and therefore, gas exchange is also influenced by gravity. However, the precise role and influence of gravity on gas exchange remains controversial (Hughes and West 2008, Glenny 2008). One method of studying this topic is to remove gravity, and investigate its effects by its absence. Prior research has highlighted the influence of microgravity on the lung and its mechanics (Frerichs *et al* 2001, Prisk *et al* 2006, Prisk 2014). The distribution of air seems to be more homogeneous in microgravity and the lung functions well in weightlessness. However, high levels of gravity, e.g. occurring during launch and atmospheric re-entry of spaceflight, have not been extensively investigated (Kaneko *et al* 1966, Anthonisen *et al* 1970, Pollock *et al* 2021). Yet, in the near future of suborbital commercial space flights, untrained passengers who are normal members of the public may likely experience such high levels of gravity (Barratt 2008). A deeper understanding of the influence of gravity on the human lung could help to avoid adverse respiratory effects during commercial space flights.

The regional distribution of ventilation can be monitored by electrical impedance tomography (EIT). This imaging modality is a non-invasive method to visualize conductivity changes in a sectional plane of the body. Regional changes of lung volume during tidal breathing lead to a significant and proportional change of

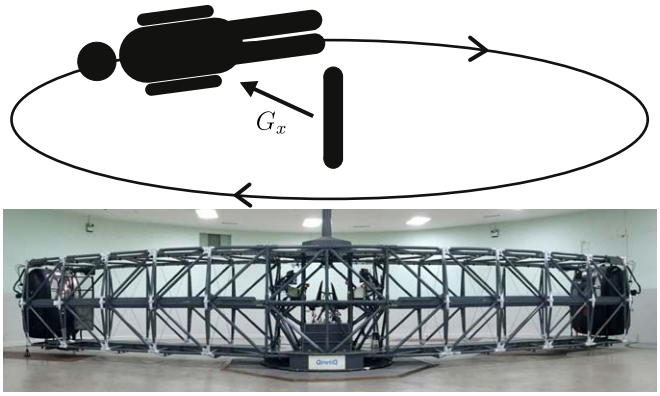

Figure 1. Participants are in a supine position in the gondola, experiencing constant earth gravity in chest-to-back direction while the gondola standstill. During centrifugation, the centrifugal force rotates the gondola in a horizontal direction (such that the base of the gondola turns in the direction of the wall). The resulting force of gravity and centrifugation aligns the axis of the gondola, so that any force G_x points form chest-to-back. The amount of G_x depends on the radial velocity of the gondola, having a minimum level of +1 G. Reproduced with permission from QinetiQ.

conductivity inside the body, which can be visualized in EIT images (Leonhardt and Lachmann 2012, Frerichs *et al* 2017).

The effects of high gravitational forces can be studied using a human centrifuge. We performed a study in a long-arm human centrifuge using magnitudes of high G-acceleration. A prior analysis focussing on gas exchange was undertaken (Pollock *et al* 2021) and found a progressively widened alveolar-arterial (A-a) oxygen gradient with increasing G_x-acceleration causing hypoxemia. Pollock also showed a reversed relative distribution of ventilation from dorsal to ventral region in combination with ventral gas trapping. Subjects reported severe breathlessness and showed a progressive increase in work of breathing and neural respiratory drive.

In addition to the preliminary analysis from Pollock, this work investigates the influence of high G_x-acceleration (in the chest-to-back direction) on ventilation, deriving different parameters from EIT images to better understand the influence of altered gravitational conditions on tidal volume, end-expiratory volume and the dynamic distribution of air inside the lung. Moreover, the study investigates the respiratory effects of simulating reduced partial pressure of inspired oxygen associated with a reduced spacecraft cabin pressure (by breathing a mildly hypoxic gas mixture) during the anticipated peak G_x load of a suborbital spaceflight.

2. Materials and methods

Astronauts are typically in a supine position during launch and re-entry of a spacecraft. In this position, the sum of acceleration and gravity vector G_x affects the body from chest-to-back (ventral to dorsal direction). This situation is mimicked using a human centrifuge shown in figure 1. The participant lies in a supine position in the centrifuge gondola. During centrifugation, participants experience a chest-to-back force ($+G_x$) as depicted in figure 1. G_x is a superposition of gravity and centrifugal-force affecting the body from ventral to dorsal. G_x induces a pleural pressure gradient. Prior research generally confirmed that the pressure gradient affects the lung and its mechanics (Kaneko *et al* 1966, Anthonisen *et al* 1970, Pollock *et al* 2021). The ventral part of the pleura has a lower pressure and is reffered to as the 'non-dependent' lung region. Consequently, the dorsal part is affected by a higher pressure and termed the 'dependent region'. In the non-dependent region, there is less mechanical compression of the alveoli compared to the dependent region.

Due to the changes in the pleural pressure gradient, the following three hypotheses were formulated: during high G_x exposure

(i) the tidal volume will decrease,

(ii) the end-expiratory volume will decrease, and

(iii) the ventilation of the non-dependent region will increase.

The following section provides detailed information about the study and participants, followed by a brief introduction to EIT to provide a better understanding of the reconstructed images. Finally, different parameters will be derived from the ventilation images.

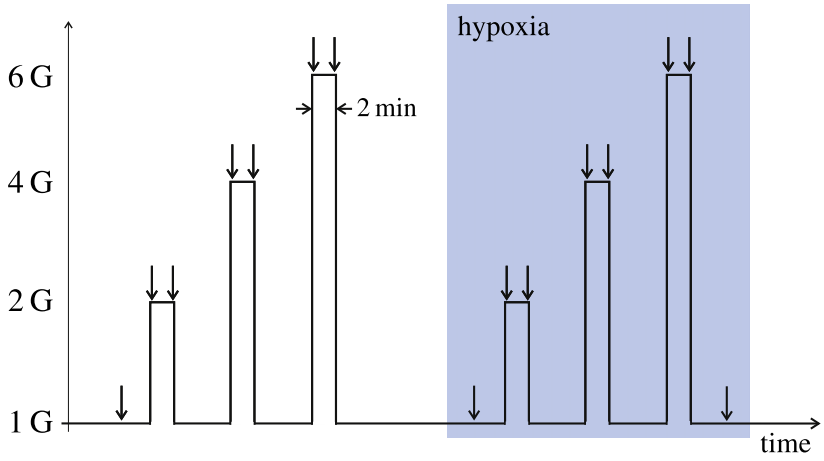

Figure 2. Different level of G_x-accelaration during the trial. Note that the order of G_x exposures was randomized between participants.

2.1. Study procedure and data selection

The study was supervised by King's College London, for Centre for Human and Applied Physiological Sciences, London, UK and carried out through QinetiQ, Farnborough, UK with approval from the QinetiQ Research Ethics Committee and King's College London Research Ethics Committee. The trial was registered under ethical approval #43032988. Ten volunteers (seven male and three female, age range: 21–40 years, mean BMI: 25.56—ST Dev: 3.8) participated in the study. The volunteers were ordinary persons with unexceptional fitness levels. All volunteers completed a medical screening questionnaire and a medical examination that classified them suitable for high-G exposures (Pollock *et al* 2021). Figure 2 schematically shows the sequence of acceleration levels.

The G_x onset rate was 0.3 G s^{-1}. In a random order, participants were exposed to +2, +4 and +6 G_x for 120 s each (at the G_x plateau) with at least 5 min break in between exposures. Note that this range of accelerations is relevant to what is typically experienced during suborbital flights (Blue *et al* 2014). In a second acceleration sequence (light-blue area), participants were asked to breath an hypoxic gas mixture with 15% fraction of inspired oxygen (FiO_2). This oxygen concentration reflects the inspired partial pressure of oxygen expected with the anticipated cabin pressure of some commercial suborbital space vehicles. The arterial oxygen saturation SpO_2 was recorded continuously at the earlobe via Powerlab 16SP and LabChart 7 (AD Instruments, Oxford, UK). 8 of 10 participants completed the runs with 15% O_2. Participants also performed a forced inspiratory vital capacity (FIVC) breathing maneuver under G_x by exhaling to residual volume followed by a 10 s long breath-hold and a 10 s long inspiration to maximal lung capacity, providing a measure of functional vital capacity. The FIVC maneuvers are represented as arrows in figure 2.

The data was recorded with a Goe-Mf II EIT device (Hahn *et al* 2002) featuring 16 Ag/AgCl gel electrodes at a rate of 33.12 frames s^{-1}. Separate EIT measurements were made at each acceleration level including a +1 G_x phase at the beginning. To allow comparisons between individuals, the calculated parameters were referenced to +1 G_x where appropriate. The intervals of tidal breathing and breathing maneuvers were selected for each participant individually with respect to the different G_x levels, to guarantee an accurate frame selection. In addition to the EIT measurements, global respiratory flow was recorded during the trials to validate the EIT data. All calculations were performed with Matlab R2017b from Mathworks and EIDORS version 3.8 (Adler and Lionheart 2006).

2.2. Electrical impedance tomography

For offline analysis, image reconstruction was performed using the GREIT solver (Adler *et al* 2009), trained on a FEM-model of the thorax with 16 electrodes (Grychtol *et al* 2012). The parameters of the algorithm were set to an image size of 64 × 64 pixels, a uniform distribution of 500 training points, a target size of 0.03 and a noise figure of 0.8. As we were interested in comparing the distribution of ventilation and volume changes of the lung to that at +1G_x, this G_x level was used as a baseline-reference for the time-differential reconstruction. Thus, the images always show relative conductivity changes compared to the mean level at +1 G_x. Furthermore, we found that other baselines lead to more distorted images, including larger ringing artifacts. The baseline- ($\bar{y}_{1G}$) and +6 G_x -interval (y_{6G}) are exemplarily labeled in the time plot of the sum of EIT measurement data $\sum y$ (figure 3). Reconstruction is given by

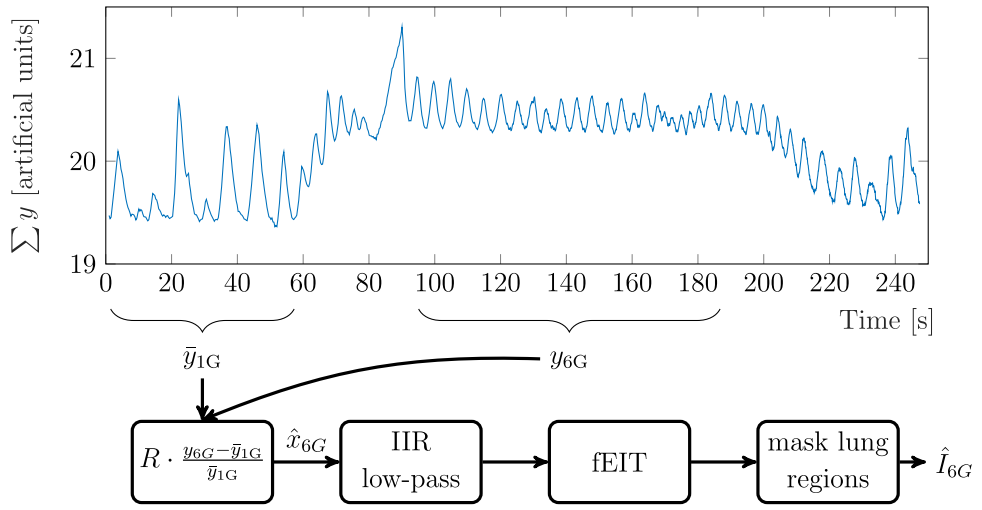

Figure 3. Flowchart of data pre-processing, exemplarily shown for a +6 G_x measurement. EIT images $\hat{x}_{6G}$ are reconstructed using +1 G_x as a baseline. Further processing includes low-pass filtering, functional EIT image calculation. Finally, a threshold-mask show almost exclusively the lung regions $\hat{I}_{6G}$.

$$\hat{x}_{nG}(m,\, n,\, i) = R \cdot \frac{y_{nG} - \bar{y}_{1G}}{\bar{y}_{1G}}, \tag{1}$$

where R is the GREIT reconstruction matrix, y_{nG} are measurement data points for a $+n$ G_x interval, $\bar{y}_{1G}$ is the averages measurement data from the mean value of a couple of breathing cycles at +1 G_x and $\hat{x}_{nG}$ represent the reconstructed images from an $+n$ G_x interval with pixels m, n and the frame number i. To reduce the influence of high-frequency artefacts, like heart-related signals, an IIR low-pass filter with a stop band frequency of 0.5 Hz was applied on the reconstructed images.

2.2.1. Functional EIT (fEIT) images

A fEIT-image describes the standard deviation of each pixel in a specific interval and, therefore, gives a measure of breathing activity. Hence, the fEIT image was calculated for each $+n$ G_x interval during tidal breathing. In the following, the fEIT images are denoted as I_{nG}.

2.2.2. Definition of lung regions

Conductivity changes in the EIT image which occur outside the lung region do not contribute to the ventilation and should be neglected as artifacts. Therefore, a mask of the lung region has been applied to $\hat{x}_{nG}$. Only pixels that fulfill

$$\hat{I}_{nG} \geqslant t \cdot \max(\hat{I}_{nG}), \tag{2}$$

where the threshold value t was empirically chosen as 0.29, were considered for the analysis.

2.2.3. Position of the electrodes

Ideally, in human EIT the electrode plane should be placed between the 5th and 6th intercostal space. For female participants, this area is directly below or on top of the breasts, depending on the anatomy. In the present study, the electrodes were always placed directly below the breasts. This led to a relatively low position of the electrode plane for some of the female participants. Regarding the EIT images from 2 out of 3 female participants, the conductivity change in the ventral area showed a conductivity change with 180° phase reversal depending on the G_x level and the breathing type. This behavior is depicted in the conductivity plot in figure 4. This phenomenon can be explained most likely by the moving diaphragm, which tends to cross the image-plane during expiration, as schematically shown in figure 4 (right). Karsten *et al* reported a similar effect for belt positions at juxta-diaphragmatic levels (Karsten *et al* 2016). The authors state that boundaries of high conductivity differences result in a negative overshoot, which can create negative impedance changes. Consequently, these impedance changes are opposite phase to the ventilation signal, and the tidal impedance variation/tidal volume ratio is reduced. Thus, comparability of conductivity changes in between different participants might not be guaranteed. For the male participants, the electrode plane was always at the appropriate level. Consequently, the three female participants were excluded from the analysis in sections 2.3.2, 2.3.3 and 2.3.4.

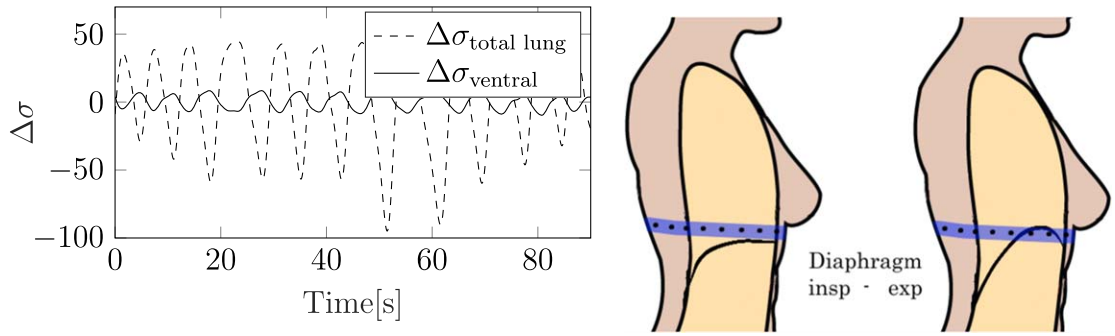

Figure 4. Left: Conductivity changes $\Delta\sigma_{\text{total lung}}$ from one of the female participants during tidal breathing (dashed). The ventral region is in 180° phase reversal (black). Right: Sketch of the potential position of diaphragm during inspiration and expiration.

2.3. Derived ventilation parameters

The following section describes the conductivity based calculation of tidal-volume, end-expiratory volume and differences between dependent and non-dependent regions. The dynamic filling and emptying behavior of the lung was also investigated to study which region of the lung contributes to the overall capacity at any given time in the breathing cycle. These parameters do not describe measured volumes. In fact, the conductivity changes of EIT images are highly correlated to the ventilation volume and therefore used for regional ventilation analysis.

2.3.1. Tidal volume index

Under the influence of high G_x, there is mechanical compression of the chest and lung. This would be expected to lead to a decrease of tidal volume, as hypothesized under (i). It has already been shown that ventilation volume changes are inversely proportional to conductivity changes during tidal breathing (Frerichs *et al* 1999). The total change of conductivity during a breathing cycle is given as:

$$\Delta\sigma_{nG} = \sum_m \sum_n \hat{x}_{nG}(m,\, n,\, i_{\max}) - \hat{x}_{nG}(m,\, n,\, i_{\min}), \tag{3}$$

where $i_{\max}$ and $i_{\min}$ are the maximum and minimum value of a breathing cycle and m, n are the pixels of the reconstructed image, respectively. To ensure that the linear relation of volume and conductivity is also applicable at high G_x, the measured flow was compared to relative conductivity changes at $+4$ G_x for one participant exemplarily. The correlation coefficient between volume and conductivity changes was 0.9963. The average total conductivity change $\Delta\bar{\sigma}_{nG}$ during an $+n$ G_x interval behaves the same as the mean tidal volume and can be calculated by:

$$\Delta\bar{\sigma}_{nG} = \frac{\sum_b \Delta\sigma_{nG}}{B}, \tag{4}$$

where b is the individual breathing cycle and B is the total number of breathing cycles in the G-phase $+n$ G. Each participant has an individual mean tidal volume and is not directly comparable to another. We note that

$$\Delta\bar{\sigma}_{nG/1G} = \frac{\Delta\bar{\sigma}_{nG}}{\Delta\bar{\sigma}_{1G}} \tag{5}$$

is the patient specific ratio of the mean conductivity change in relation to $+1$ G_x level. Thus, $\Delta\bar{\sigma}_{nG/1G}$ is independent of the absolute tidal volume of each patient.

2.3.2. End-expiratory volume index

The ventilation volume changes have a linear relation to the conductivity change, as shown in the previous paragraph. Consequently, a change of the mean end-expiratory conductivity $\overline{EEC}_{nG/1G}$ is inversely proportional to a change in the end-expiratory volume. The calculation of the ratio from $+n$ G_x to $+1$ G_x is equivalent with the calculation above:

$$\bar{\sigma}_{nG} = \frac{\sum_b \sum_m \sum_n \hat{x}_{nG}(m,\, n,\, i_{\max})}{B}, \tag{6}$$

$$\overline{EEC}_{nG/1G} = \frac{\bar{\sigma}_{nG}}{\bar{\sigma}_{1G}}. \tag{7}$$

$\overline{EEC}_{nG/1G}$ will be used to validate hypothesis ii, which suggests a decrease of the end-expiratory volume.

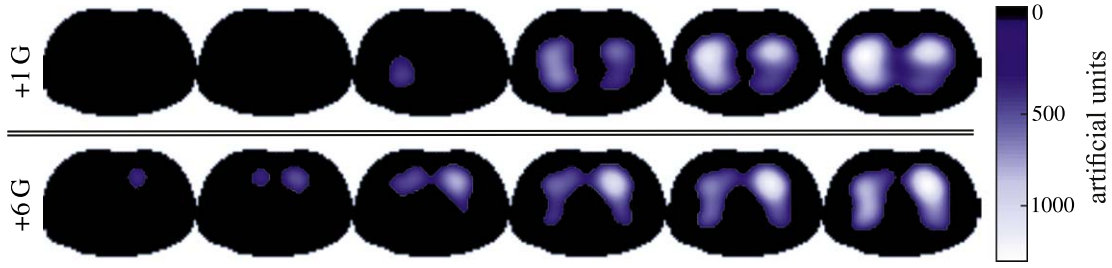

Figure 5. Exemplary set of EIT frames of the inspiration-cycle at +1 G_x (top row) and at +6 G_x (bottom row).

2.3.3. Shifts in ventilation

In the history of EIT it has been found useful to compare the breathing activity in different regions of the lung (Frerichs *et al* 2017). Because we are interested in differences between ventral and dorsal regions, the image is divided in a non-dependent region I_{nG}^{ventral} and a dependent region I_{nG}^{dorsal}, which comprise the upper and lower half of the image, respectively. The ratio of ventral breathing activity at $+n$ G_x in relation to +1 G_x is given as

$$BA_{nG/1G}^{\text{ventral}} = \frac{\sum\sum I_{nG}^{\text{ventral}}}{\sum\sum I_{nG}} \cdot \frac{\sum\sum I_{1G}}{\sum\sum I_{1G}^{\text{ventral}}}, \tag{8}$$

which can be compared between participants, due to the reference to the whole lung I_{nG}.

2.3.4. Dynamic behavior of the lung

The ratio of ventilation in dependent and non-dependent regions, presented in the previous section, is an average of regional ventilation activity during a G_x-interval. For a deeper understanding of the dynamic behavior, FIVC breathing maneuver were investigated frame by frame. The image sequence $\hat{x}_{nG}^{BM}$ of a breathing maneuver contains the temporal and regional change of lung volume. The dynamic behavior shows how much the ventilation of a particular region contributes to the total ventilation during a breathing cycle. This might be helpful in understanding how the lung mechanics are influenced by G_x-acceleration. An approach to study the emptying behavior of the lung has been presented by Frerichs *et al* (2001). This method was adapted for the filling behavior under high G_x.

The analysis was performed onto the maximal FIVC breathing maneuvers to include the activity of the intercostal muscle (musculi intercostales) and the diaphragm. A specific mask with a threshold of 0.3 of the maximum was applied to each frame of the unfiltered EIT images $\hat{x}_{nG(BM)}$, see equation (2). An exemplary inspiration sequence of masked EIT images, shown in figure 5, visualizes a shift of ventilation to the non-dependent region. Additionally, the inspiration starts significantly earlier in the non-dependent region at +6 G. All participants showed similar results with different magnitudes and lung shapes. To quantify the effect of shift in ventilation we introduce the conductivity change during inspiration (CCI) and expiration (CCE), which is calculated as followed. The masked EIT images are used to derive the ratio of lung volume continuously during the breathing maneuver in the ventral and dorsal region, respectively. For each region, all pixels were added differentiating dependent and non-dependent regions. Each of the curves was normalized by dividing it by the maximum absolute value of the image. Consequently, the CCI and CCE was calculated by

$$CCI_{\text{ROI}} = \frac{\sum_n\sum_m \hat{x}_{nG(\text{BM})}^{\text{ROI}}(i_{\text{insp}})}{\max(\hat{x}_{nG(\text{BM})}^{\text{ROI}}(i_{\text{insp}}))},\ CCE_{\text{ROI}} = \frac{\sum_n\sum_m \hat{x}_{nG(\text{BM})}^{\text{ROI}}(i_{\text{exp}})}{\max(\hat{x}_{nG(\text{BM})}^{\text{ROI}}(i_{\text{exp}}))}, \tag{9}$$

where ROI is either the ventral or dorsal region and i_{insp} and i_{exp} are the frames from inspiration and expiration of the breathing maneuver, respectively. For each part of the cycle (inspiration and expiration), the normalized curve of each region was plotted against the normalized curve of the total lung. The standard deviation of the distances d between the dependent and the non-dependent curves will be used as an evaluation parameter

$$S_{insp/exp} = \sqrt{\frac{\sum(d-\bar{d})^2}{\#i_{\text{insp/ exp}}}}, \tag{10}$$

where $\#i$ describes the number of frames of the inspiration or expiration interval.

2.4. Statistical analysis

All numerical results are visualized in boxplots with a maximum whisker length of 1.5 of the interquartile range. A two-way ANOVA was conducted to test the influence of the acceleration effect and the FiO_2 on the calculated

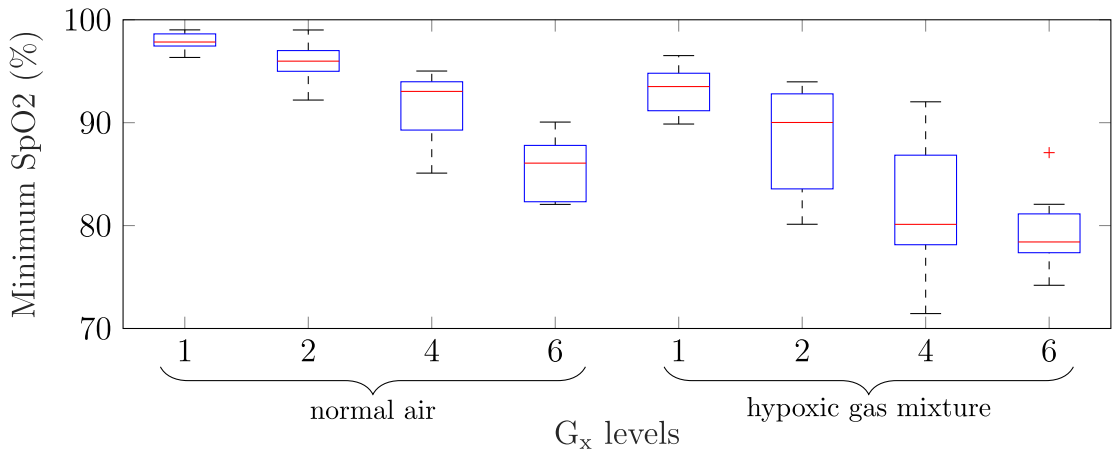

Figure 6. Boxplot of minimum SpO_2. The mean minimum SpO_2 decreased with increasing $+G_x$ level and was lower under mildly hypoxia conditions.

parameters. The first factor of the ANOVA is the G_x level group and the second factor is the normal air and hypoxic group. $p < 0.05$ has been considered as significant.

3. Results

3.1. Arterial oxygen saturation

SpO_2 of each participant was monitored at the earlobe and has recently been published (Pollock *et al* 2021). The results are shown in figure 6 to aid interpretation of the ventilation indices reported in this publication. The minimum SpO_2 of each participant was the lowest SpO_2 that was observed during each G exposure and is significantly different between the G-levels ($p < 0.001$). The mean value of the minimum SpO_2 decreased from 98% at $+1$ G_x to 86% at $+6$ G_x for normal air. Participants breathing the hypoxic gas mixture experienced a similar reduction of SpO_2. However, the minimum SpO_2 of the hypoxic group was already 5% lower at $+1$ G_x, and we observed a significant difference in SpO_2 between normal air and hypoxic ($p < 0.001$).

3.2. Derived ventilation indices

3.2.1. Decrease in tidal volumes

As exemplarily shown in section 2.3.1, conductivity changes have an inversely proportional relationship to volume changes in the lung. Consequently, the influence of gravity on the amplitude of the conductivity changes was investigated. Figure 7 represents the mean amplitude of the conductivity changes of the total lung during tidal breathing $\Delta\bar{\sigma}_{nG/1G}$.

The mean conductivity change obtained from each interval was normalized to the mean conductivity change of the cycles in $+1$ G_x from the same measurement. We note that the results at $+2$ G_x and $+4$ G_x did not differ in a significant way from $+1$ G_x ($p = 0.75$ and $p = 0.63$). However, at $+6$ G_x the tidal conductivity change was half of the tidal-value at $+1$ G_x. Under low oxygen conditions (hypoxic gas mixture), the inter-individual variability was reduced, especially at $+4$ G_x. The most interesting aspect of figure 7 is a significant decrease of tidal conductivity change with increasing G_x ($p = 0.024$). However, there was no significant difference between normal air and hypoxia ($p = 0.457$). Results during FIVC breathing maneuvers, $\bar{\sigma}_{BM}$, showed the same behavior with a lower variability, especially at $+4$ G_x (not shown).

3.2.2. Increase of end-expiratory volume

The second parameter of the ventilation analysis was the mean relative end expiratory conductivity ($\overline{EEC}_{nG/1G}$) during tidal breathing, which corresponds to the functional residual capacity. Because absolute values are not comparable between participants, each value was related to $+1$ G_x. As shown in figure 7, the value of the $\overline{EEC}_{nG/1G}$ decreased with increasing G_x exposure. There was a significant effect of G level with ($p < 0.001$). However, the large variations at $+4$ G_x were smaller in the $+4$ G_x hypoxic group. Also, there was a significant difference between the groups with normal air and hypoxia ($p < 0.001$).

A lower conductivity can be interpreted as air inside the lung. In this case, the end-expiratory volume increases under $+G_x$, which points to gas trapping in the alveoli. Under high $+G_x$ the $\overline{EEC}_{nG/1G}$ decreased below zero. The negative sign corresponds to values that are bellow the baseline.

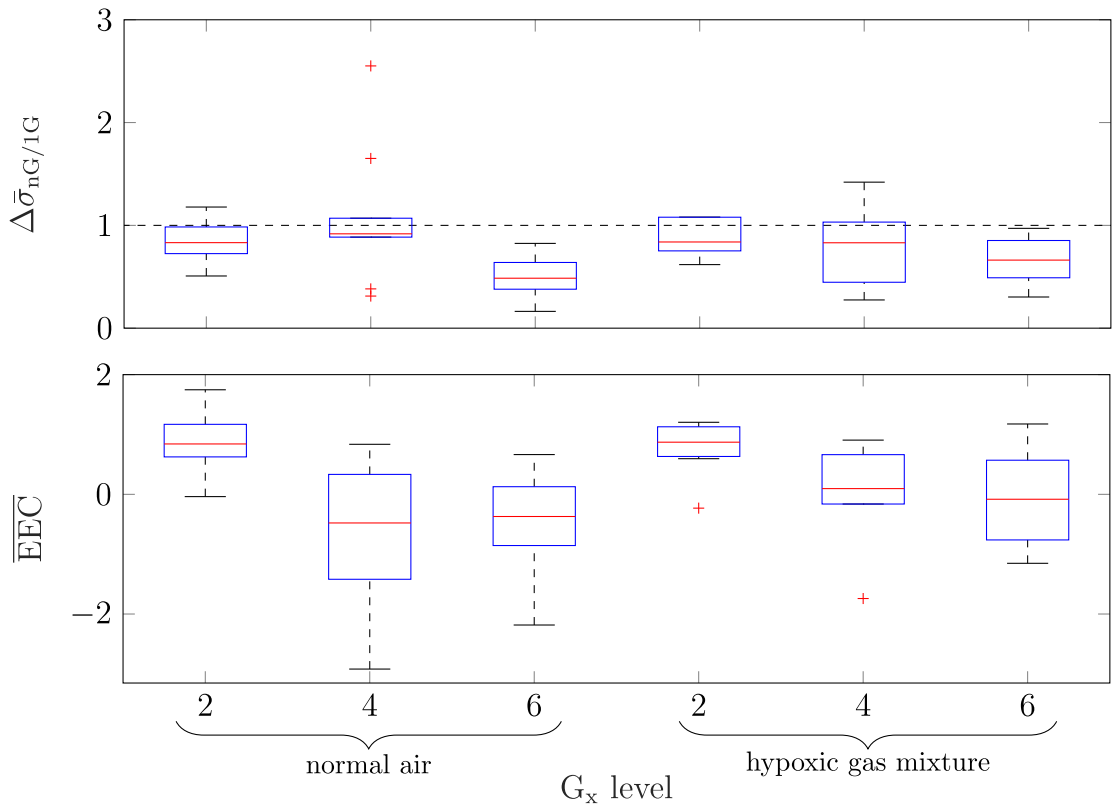

Figure 7. Top: Boxplot of the ratio between the mean conductivity changes during tidal breathing at each $+G_x$ level and the reference value of $+1$ G_x of each file including all ten participants for normal air and eight participants for hypoxia (two participants did not finish hypoxic runs). Bottom: Boxplot of the ratio between the mean end-expiratory conductivity values during tidal breathing and the reference value of $+1$ G_x of each file including seven male participants. The reference is at $+1$ G_x for $\Delta\bar{\sigma}_{1G/1G} = 1$ and marked with a dashed black line.

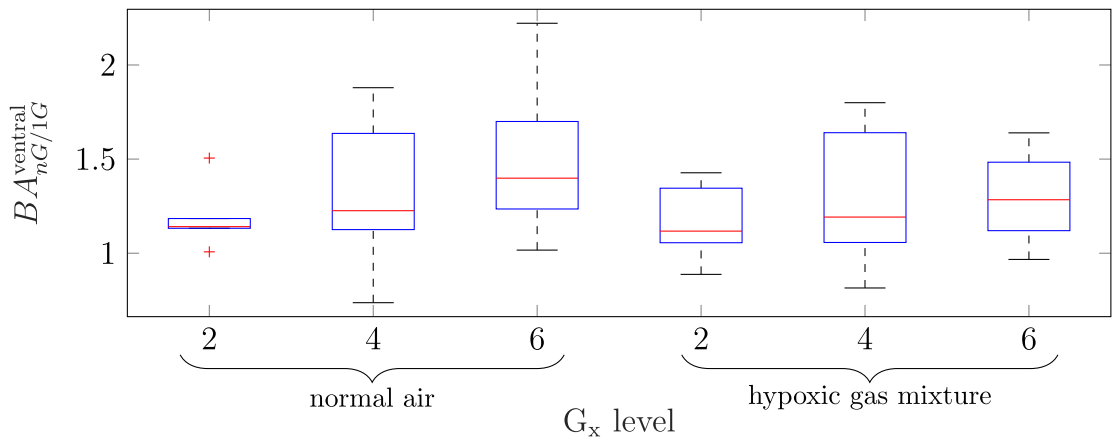

Figure 8. Proportion of ventilation occurring in the ventral region of the lung at different levels of Gz when breathing normal air and hypoxic gas mixture, from $n = 7$ male participants.

3.2.3. Shifts in ventilation

The variable $BA^{ventral}_{nG/1G}$ represents the amount of ventral ventilation in relation to $+1$ G_x (figure 8). With increasing G_x level, the distribution of ventilation shifted towards the ventral region. This effect was more pronounced during tidal breathing compared with FIVC breathing maneuvers. Variability between participants also increased with $+G_x$. The highest variability was observed at $+6$ G_x. At $+6$ G_x, one participant showed a complete shift of ventilation to the ventral region. However, the $+4$ G_x and $+6$ G_x hypoxic group had less variation compared to normal air. There was a significant difference between the G_x level groups with $p = 0.018$. There was also a significant difference between the groups with normal air and hypoxia ($p < 0.001$).

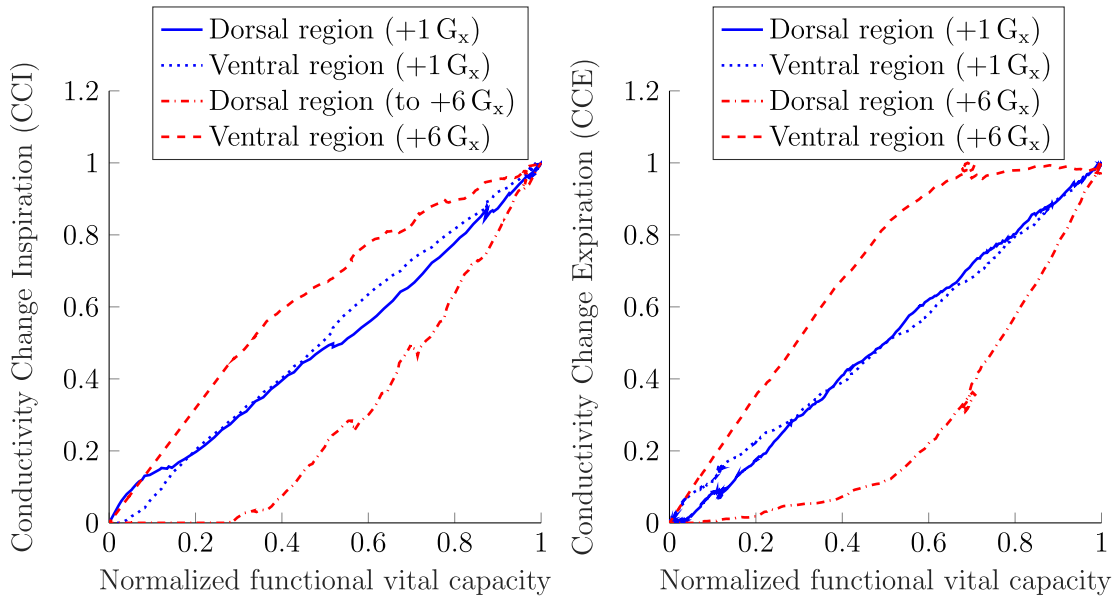

Figure 9. Example of filling (left) and emptying (right) behavior curves of the ventral (non-dependent) and dorsal (dependent) regions for +1 G_x and +6 G-exposures with normal air.

3.2.4. Dynamic behavior of the lung

To quantify the dynamic behavior of the lung, the filling and emptying behavior was investigated considering the dorsal and ventral regions as dependent and non-dependent regions, respectively. Figure 9 provides illustrative examples of the ventral and dorsal regions for the filling behaviour in the top graph and for the emptying behaviour below.

The *x*-axis represents the normalized capacity of the total lung, meaning the sum of both the dependent and non-dependent regions. The *y*-axis represents the proportion of the maximum capacity that can be reached in that particular region of interest. It is important to note that the interpretation of each breathing cycle must be performed separately, which means that the values between dependent and non-dependent regions are not complementary. For instance, consider the CCE value at +6 G_x in figure 9: when the whole lung is filled to 40% of the total capacity, the ventral region is filled up to 68% of its own capacity. However, the dorsal region reaches only 7.1% of it's own capacity.

In the case of +1 G_x, both regions tend to perform similarly with almost linear behavior. For +6 G_x the filling of the ventral (non-dependent) region starts faster, while towards the end of the inspiration the curve flattens. In contrast, the dorsal (dependent) regions show a later start of the filling and fills faster towards the end. On the other hand, the emptying of the dependent region occurs considerably faster compared to the non-dependent one. For some participants, the effect of +G_x was pronounced and it induced almost a complete shift of the lung volume towards the ventral region. This means that no ventilation activity was detected in the dorsal region and consequently the ventral region showed a linear behaviour. For these cases, the curvature coefficient from Frerichs *et al* (2001) was not applicable. However, for +4G_x and +6 G_x (in both normal air and hypoxic gas) the variability between the upper and the lower quartile increased. Because of this, the distance between all points of the dependent and non-dependent curves was calculated for each participant, and then summarized in one single parameter $S_{\mathrm{insp/exp}}$ by computing the standard deviation of the distances for each pair of curves in relation to +1 G_x, according to equation (10). The box plots for inspiration and expiration is shown in figure 10.

The standard deviation of the distance between the dependent and non-dependent region increased significantly at higher G_x level ($p_{\mathrm{insp}} < 0.001$ and $p_{\mathrm{exp}} = 0.031$). Also, the variance in figure 10 increased with the G_x level, which could be a result of differences between participants in respiratory muscle strength. However, at high G_x the dorsal region had a different response as the ventral and the difference between both regions increased with the G_x level. For the inspiration, no significant differences were found between normal air and hypoxic gas ($p_{\mathrm{insp}} = 0.07$). In contrast, the distance variations showed a significant difference in the expiration between normal air and hypoxic gas ($p_{\mathrm{exp}} = 0.002$).

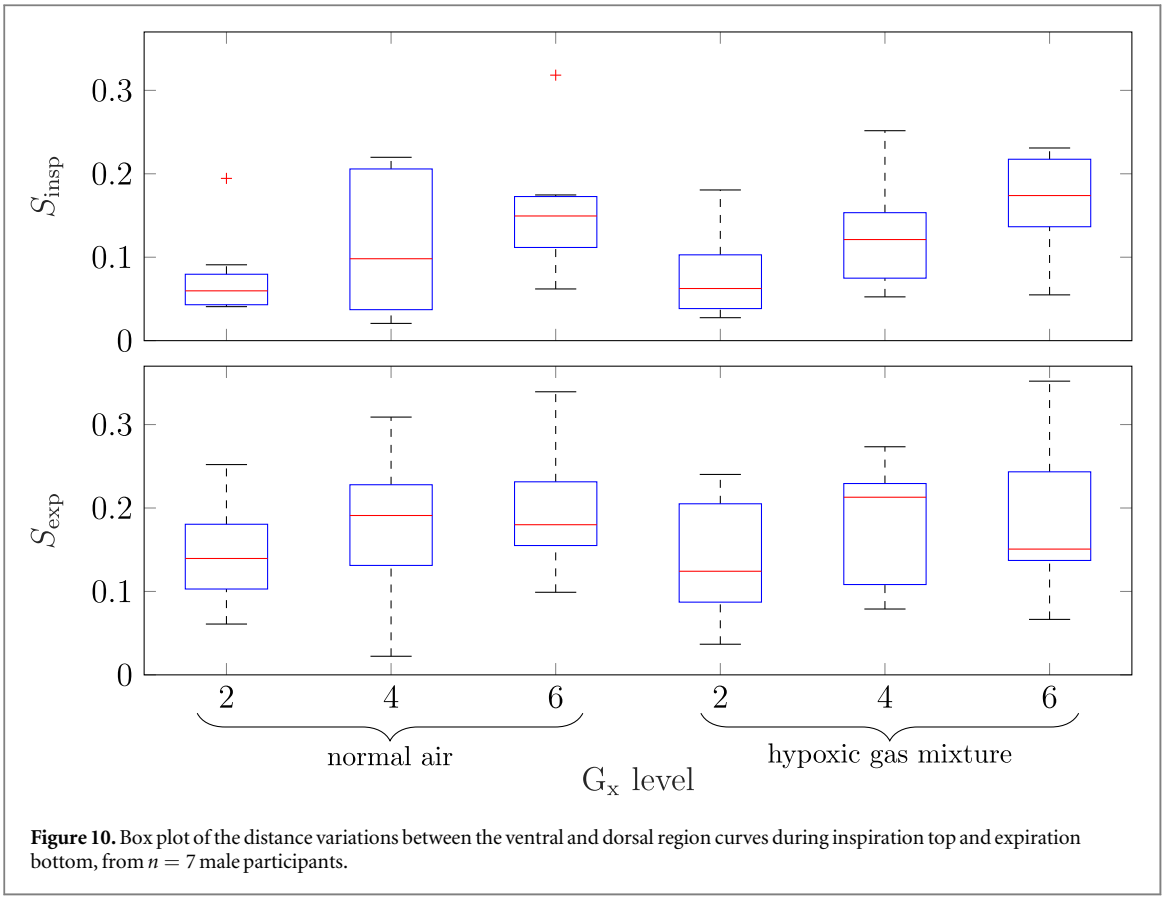

Figure 10. Box plot of the distance variations between the ventral and dorsal region curves during inspiration top and expiration bottom, from $n = 7$ male participants.

4. Discussion

In this study, seven male and three female participants were exposed to +2, +4 and +6 G_x in the chest-to-back direction to study the magnitude of acceleration experienced during launch and re-entry in suborbital spaceflight. In general, increasing G_x levels result in mechanical compression of the thorax. Therefore, we expected a decrease in tidal volume with increasing G_x level (hypothesis i). Indeed we found a decrease in conductivity change during tidal breathing for an increasing G_x level, supporting this hypothesis. A reduced tidal volume could lead to reduced gas exchange and a reduced SpO_2 value. The minimum recorded SpO_2 decreased along with the tidal conductivity change with increasing G_x level.

Consequently, in hypothesis ii we assumed that lung capacity is restricted due to higher G_x levels, which results in a decrease of the end-expiratory volume. The mean relative end-expiratory conductivity ($\overline{EEC}_{nG/1G}$) decreased, which meant the end-expiratory volume increased. This phenomenon can be explained physiologically with a pressure difference inside the lung. Due to high G_x level, the pleural pressure increases in the dependent (dorsal) region of the lung. Therefore, the emptying starts in the dorsal area. When the pleural pressure exceeds airway pressure, the airways collapse and air is trapped mainly in the ventral region of the lung (Glaister 1970b).

Finally, we observed a shift of ventilation towards the non-dependent (ventral) region, which supports hypothesis iii. In addition, the analysis of the dynamic behavior during a breathing cycle of the lung reveals that the dorsal region empties faster than the ventral region. When the airways collapse, air is still inside the ventral region leading to an increase of the end-expiratory volume. This result opposes hypothesis ii.

Another important finding was that the filling started in the ventral area and resulted in an increased maximum volume for this region. This phenomenon can be explained by the pleural pressure difference, which is smaller in the non-dependent (ventral) region of the lung (Glaister 1970a, 1970b). Consequently, in the dorsal region the alveoli are more compressed and more difficult to fill. However, once they are opened, the relatively small end-value is reached quickly. Accordingly, the emptying starts in the dorsal area, where the pressure is the highest.

In general, all derived ventilation indices and the minimum SpO_2 value showed a high inter-individual variability at +4 G_x. As participants reported a significant increase in breathing effort at +4 G_x and higher, we believe participants tried to actively overcompensate the experienced chest pressure with increasing thoracic breathing effort. These results may therefore be quiet dependent on the physical conditioning of each

participant. At +6 G_x, participants reported difficulty breathing and measurements had less variability (compared to +4 G_x) potentially due to chest compression resulting in differences in physique might being less relevant.

EIT measurements with a juxta-diaphragmatic belt position may lead to artifacts and phase shifts caused by diaphragmatic movements (Karsten *et al* 2016). High G_x compresses the lower abdomen so that the diaphragm might be pushed to a more cranial position during exhalation. Considering the relatively low EIT electrode position in female participants, the diaphragm most probably has reached into the ventral area of the EIT images. Thus, the linear relation of conductivity change and ventilation was distorted. The female participants were therefore excluded from most of the analysis.

In future studies, simultaneous measurements should be made from a second electrode plane placed above the breast. A reconstruction on two levels might show the influence of gravitational force in the position of the diaphragm. In addition, a second electrode plane would enable the usage of non-linear 3D-EIT reconstruction algorithms (Liu *et al* 2016). Another aspect of the study was the influence of reduced oxygen on ventilation. The reduced FiO_2 leads to a reduced SpO_2, and the results tend to show a smaller variability between participants for increasing G_x levels. Apart from that, no other significant influences of reduced FiO_2 on the ventilation were found for the derived parameters.

5. Conclusion

The present study was designed to determine the effect of high gravity exposure in the chest-to-back direction on the human lung. More specifically, regional volume changes of ventilation were monitored with EIT as part of a human centrifuge trial. The shift of ventilation, the emptying behavior and the end-expiratory volume reveal enclosed air in the ventral region at the end of expiration (gas trapping). The "trapped air" reduces the amount of active air contributing to gas exchange and contributes to impairment of ventilation/perfusion matching and hypoxaemia. This work contributes to existing knowledge of Pollock *et al* (2021) by providing insights into the dynamic behavior of regional lung ventilation as measured by EIT. At +6 G_x, all participants were affected similarly by the acceleration level. However, at +4 G_x, participants appeared to compensate variably for the effects of hypergravity with muscle force, depending on the individual physical conditions. This inter-individual variability makes these findings less generalizable to define a strict relationship between gravity and tidal volume. Future work should focus on this relationship and include +2 G_x and +4 G_x phases of 3 min, evaluated in the last minute of the G-phase. This might reduce the inter-individual variability and reveal a more clear correlation between G-level and tidal-volume change.

Acknowledgments

The authors would like to thank the study participants, centrifuge engineers and medical officers for their commitment and effort in making this study possible.

Financial Disclosure Statement: this work was supported by a grant from the UK Space Agency (ST/R006113/1). The authors have no competing interests to declare.

ORCID iDs

Tobias Menden https://orcid.org/0000-0003-2400-2978
Ross D Pollock https://orcid.org/0000-0002-3184-8253
Caroline Jolley https://orcid.org/0000-0003-3538-2451
Thomas G Smith https://orcid.org/0000-0002-5197-5030
Steffen Leonhardt https://orcid.org/0000-0002-6898-6887
Marian Walter https://orcid.org/0000-0003-4137-5370

References

Adler A *et al* 2009 GREIT: a unified approach to 2D linear EIT reconstruction of lung images *Physiol. Meas.* **30** S35–55
Adler A and Lionheart W R B 2006 Uses and abuses of EIDORS: an extensible software base for EIT *Physiol. Meas.* **27** S25–42
Anthonisen N R, Robertson P C and Ross W R 1970 Gravity-depende sequential emptying of lung regions *J. Appl. Physiol.* **28** 589–95
Barratt M R 2008 Physical and Bioenvironmental Aspects Of Human Space Flight *Principles of Clinical Medicine for Space Flight* ed M R Barratt and S L Pool (New York,NY: Springer) pp 3–26 Chap. 279780387988429
Blue R S, Pattarini J M, Reyes D P, Mulcahy R A, Garbino A, Mathers C H, Vardiman J L, Castleberry T L and Vanderploeg J M 2014 Tolerance of centrifuge-simulated suborbital spaceflight by medical condition *Aviation Space Environ. Med.* **85** 721–9

Frerichs I et al 2017 Chest electrical impedance tomography examination, data analysis, terminology, clinical use and recommendations: Consensus statement of the TRanslational EIT developmeNt stuDy group *Thorax* **72** 83–93
Frerichs I, Dudykevych T, Hinz J, Bodenstein M, Hahn G and Hellige G 2001 Gravity effects on regional lung ventilation determined by functional EIT during parabolic flights *J. Appl. Physiol.* **91** 39–50
Frerichs I, Hahn G and Hellige G 1999 Thoracic electrical impedance tomographic measurements during volume controlled ventilation-effects of tidal volume and positive end-expiratory pressure *IEEE Trans. Med. Imaging* **18** 764–73
Glaister D H 1970a Distribution of pulmonary blood flow and ventilation during forward (plus Gx) acceleration *J. Appl. Physiol.* **29** 432–9
Glaister D H 1970b *The Effects of Gravity and Acceleration on the Lung* 1 edn (London: Technivision Services) https://apps.dtic.mil/dtic/tr/fulltext/u2/882903.pdf978-0851020273
Glenny R 2008 Counterpoint: gravity is not the major factor determining the distribution of blood flow in the healthy human lung *J. Appl. Physiol.* **104** 1533–5
Grychtol B, Lionheart W R B, Bodenstein M, Wolf G K and Adler A 2012 Impact of model shape mismatch on reconstruction quality in electrical impedance tomography *IEEE Trans. Med. Imaging* **31** 1754–60
Hahn G, Dudykevych T, Frerichs I, Thiel F and Hellige G 2002 A high performance electrical impedance tomography (EIT) system clinical evaluation studies and space application *13th Int. Conf. on Electrical Bioimpedance and the 8th Conf. on Electrical Impedance Tomography (Graz, Austria, August 29th - September 2nd 2007)* ed Scharfetter Hermann and Merwa Robert (Berlin: Springer) 978-3-540-73841-1
Hughes M and West J B 2008 Point:Counterpoint: Gravity is/is not the major factor determining the distribution of blood flow in the human lung *J. Appl. Physiol.* **104** 1531–3
Kaneko K, Milic-Emili J, Dolovich M B, Dawson A and Bates D V 1966 Regional distribution of ventilation and perfusion as a function of body position *J. Appl. Physiol.* **21** 767–77
Karsten J, Stueber T, Voigt N, Teschner E and Heinze H 2016 Influence of different electrode belt positions on electrical impedance tomography imaging of regional ventilation: a prospective observational study *Crit. Care* **20** 1–10
Leonhardt S and Lachmann B 2012 Electrical impedance tomography: The holy grail of ventilation and perfusion monitoring? *Intensive Care Med.* **38** 1917–29
Liu D, Kolehmainen V, Siltanen S, Laukkanen A M and Seppanen A 2016 Nonlinear difference imaging approach to three-dimensional electrical impedance tomography in the presence of geometric modeling errors *IEEE Trans. Biomed. Eng.* **63** 1956–65
Pollock R D et al 2021 Pulmonary effects of sustained periods of high-G acceleration relevant to suborbital spaceflight *Aerosp. Med. Hum. Performance* https://kclpure.kcl.ac.uk/portal/files/149911578/Author_accepted_manuscript_March_2021.pdf
Prisk G K 2014 Microgravity and the respiratory system *Eur. Respiratory J.* **43** 1459–71
Prisk G K, Fine J M, Cooper T K and West J B 2006 Vital capacity, respiratory muscle strength, and pulmonary gas exchange during long-duration exposure to microgravity *J. Appl. Physiol.* **101** 439–47